CrIS Full Resolution Processing and Validation System for JPSS

Yong Chen[1], Yong Han[2], Denis Tremblay[3], Likun Wang[1], Xin Jin[4], and Fuzhong Weng[2]

[1]Earth System Science Interdisciplinary Center, University of Maryland, College Park, MD
[2]NOAA Center for Satellite Applications and Research, College Park, MD
[3]Science Data Processing Inc., Laurel, MD
[4]ERT, Laurel, MD

Abstract

Based on the Cross-track Infrared Sounder (CrIS) Algorithm Development Library (ADL), CrIS full resolution Processing System (CRPS) has developed to generate the full spectral resolution (FSR) Sensor Data Record (SDR). We are also developing the CrIS FSR SDR Validation System (CRVS) to quantify the CrIS radiometric and spectral accuracy, since they are crucial for improving its data assimilation in the numerical weather prediction, and for retrieving atmospheric trace gases. In this study, CrIS full resolution SDRs are generated from CRPS using the data collected from FSR mode of Suomi National Polar-orbiting Partnership Satellite (S-NPP), and the radiometric and spectral accuracy are assessed by using the Community Radiative Transfer Model (CRTM) and European Centre for Medium-Range Weather Forecasts (ECMWF) forecast fields. The biases between observation and simulations are evaluated to estimate the FOV-2-FOV variability for clear sky over ocean. Double difference method and Simultaneous Nadir Overpass (SNO) method are also used to assess the CrIS radiance consistency with well-validated IASI. Two basic frequency validation methods (absolute and relative spectral validations) are used to assess the CrIS spectral accuracy. Since CrIS shortwave infrared (SWIR) band has four times higher resolution than normal mode, it makes possible to use SWIR band to assess the spectral accuracy. All three CrIS bands and 9 field of views (FOVs) spectral evaluations are done separately for clear scenes over oceans at nadir (the 15th and 16th field of regards (FORs)). Results show that CrIS SDRs from FSR have similar radiometric and spectral accuracy as those from normal mode.

1. Introduction

The Cross-track Infrared Sounder (CrIS) on Suomi National Polar-orbiting Partnership Satellite (S-NPP) is a Fourier transform spectrometer. In normal mode (mission mode), CrIS measures the spectral bands from 650 to 1095 cm^{-1} (long-wave IR band, LWIR), 1210 to 1750 cm^{-1} (mid-wave IR band, MWIR), and 2155 to 2550 cm^{-1} (short-wave IR band, SWIR) with spectral resolutions of 0.625 cm^{-1}, 1.25 cm^{-1} and 2.5 cm^{-1}, respectively. It provides a total of 1305 channels for sounding the atmosphere. CrIS can also be operated in the full spectral resolution (FSR) mode, in which the MWIR and SWIR band interferograms are recorded with the same maximum path difference as the LWIR band and with spectral resolution of 0.625 cm^{-1} for all three bands (total 2211 channels). Table 1 lists the CrIS normal and full resolution channel characteristics. NOAA plans to operate CrIS in FSR mode in December 2014 for SNPP and the Joint Polar Satellite System (JPSS) in the future in order to improve the retrieval accuracy of water vapor, carbon monoxide, carbon dioxide and methane. Up to date, the FSR mode has been commanded three times in-orbit (02/23/2012, 03/12/2013, and 08/27/2013). CrIS normal mode SDR will be

operationally generated from the current Interface Data Processing Systems (IDPS) with the FSR Raw Data Record (RDR) truncation module. Based on CrIS Algorithm Development Library (ADL), a prototype version of CrIS full resolution Processing System (CRPS) has been developed to generate the FSR Sensor Data Record (SDR) offline. We also are developing the CrIS FSR SDR Validation System (CRVS) to quantify the CrIS radiometric and spectral accuracy, since they are crucial for improving its data assimilation in the numerical weather prediction, and for retrieving atmospheric trace gases.

Table 1. CrIS normal and full resolution channel characteristics

Frequency Band	Spectral Range (cm^{-1})	Number of Channel (unapodized channel)	Spectral Resolution (cm^{-1})	Effective MPD (cm)
LWIR	650 to 1095	713 (717[b])	0.625	0.8
MWIR	1210 to 1750	433 (437[b])	1.25	0.4
		865[a] (869[b])	0.625	0.8
SWIR	2155 to 2550	159 (163)	2.5	0.2
		633[a] (637[b])	0.625	0.8

a: full resolution channels
b: number of spectral bins with two extra data points at each end of the spectrum included in the SDR product for applications of an external spectral apodization

2. CrIS FSR Processing System (CRPS)

The current FSR SDR processing system is based on the scheme for the current operational CrIS normal mode SDR processing system, which is shown in Figure 1. CrIS SDR Algorithm product comprises the radiance, NEdN (noise), geolocation, and data quality flags. The spectral resampling (to user's grid) step is performed before the instrument line shape (ILS) correction which comprises the self-apodization removal. The calibration approach does the radiometric calibration first, and then applies the correction matrix operator (CMO) which includes the post calibration filter, spectral resampling, self-apodization removal and residual ILS removal. The CrIS SDR algorithm data flow is currently being reevaluated.

3. CrIS Radiometric Accuracy Assessment

The normal mode CrIS SDR radiometric and spectral accuracy assessments can be found at [Han et al., 2013; Strow et al., 2013; Tobin et al., 2013]. In this study, we focus on the assessments of the radiometric and spectral accuracy from the full resolution CrIS SDR, which are generated from ADL with updated non-linearity coefficients, ILS parameters, and periodic sinc function for CMO using August 27-28, 2013 full spectral resolution RDR data.

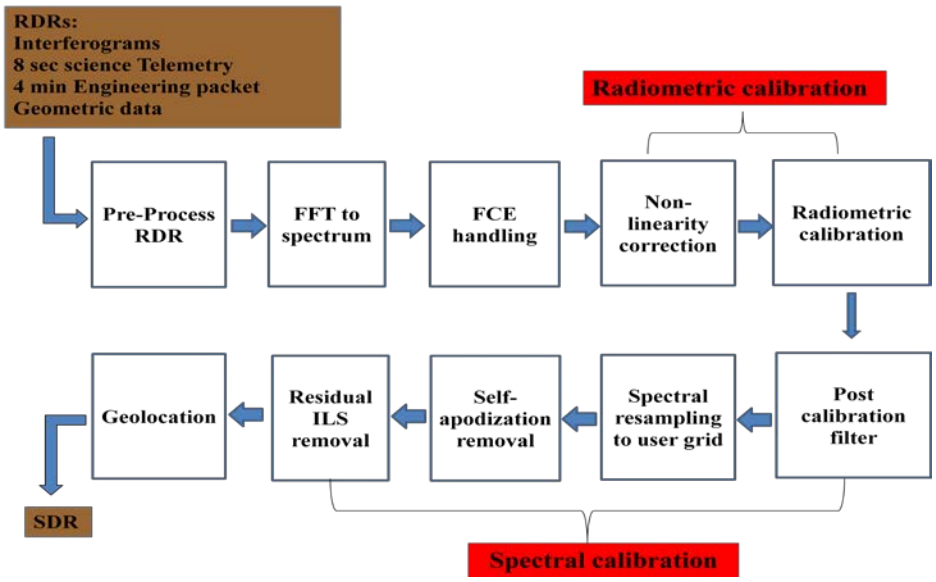

Figure 1. Scheme for the CrIS SDR radiometric and spectral calibrations.

3.1 Comparison to Forward Model Simulation

We use three assessment approaches to evaluate the CrIS radiometric accuracy. The first approach is to calculate the differences between the CrIS observations and forward simulations (O-S).

$$\Delta BT = BT_{obs} - BT_{CRTM} \tag{1}$$

The accuracy of this approach is dependent on the accuracy of the forward model and its atmospheric profiles and surface conditions. In this study, to make sure the simulated radiances having high accuracy, we use Community Radiative Transfer Model (CRTM) [Han et al., 2006; Chen et al., 2008, 2010, and 2012] and the atmospheric profiles (pressure, temperature, water vapor, and ozone) from European Center for Medium-range Weather Forecasts (ECMWF) analysis/forecast model data over oceans. The sea surface temperatures (SSTs) are from ECMWF analysis model, the sea surface emissivity by Wu and Smith [1997], and shortwave infrared sea surface reflection model by Chen et al. [2013a]. The effects of possible contamination by clouds or spatially varying humidity in the CrIS observations are detected by using the hyper-spectral IR cloud detection algorithm [McNally and Watts, 2003] coupled with CRTM. The SDR dataset were evaluated to estimate the FOV2-2-FOV variability by removing the mean bias between observations and CRTM simulations over the nine FOVs at each FOR for clear sky over ocean. Figure 2 shows that FOV-2-FOV variability is about 0.05 K or better in the LWIR and MWIR except for MWIR FOV 7 which has an out of family large relative bias around 0.3 K at some channels (a known issue since pre-launch tests). For shortwave band, the variability is slight larger, about 0.1 K and some channel can reach about 0.3 K. The small FOV to FOV relative radiometric variability indicates that the satellite data assimilation systems can use any FOV observation with about the same bias.

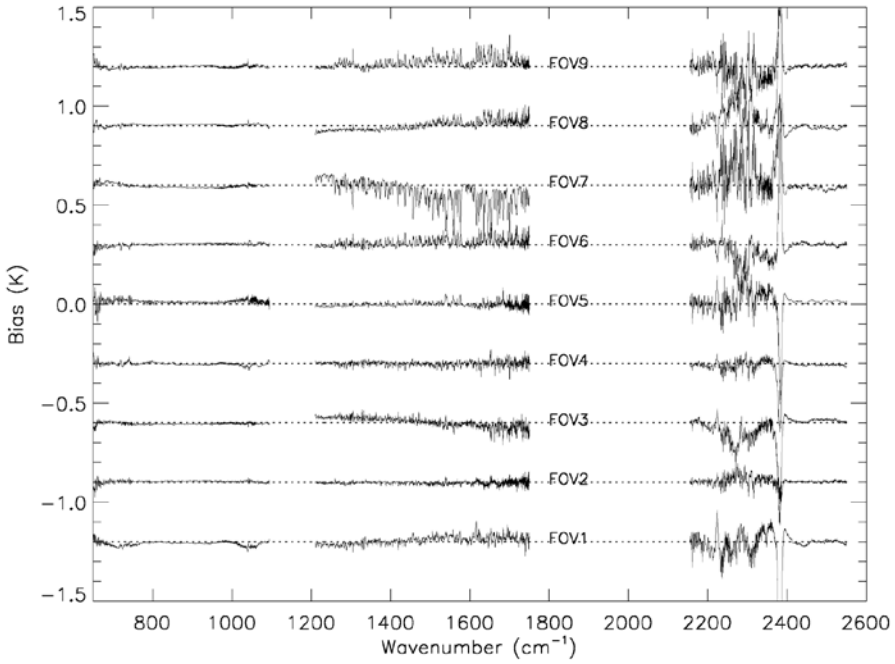

Figure 2. The nine FOV to FOV (FOV-2-FOV) relative radiometric variability by removing the mean bias between observations and CRTM simulations at nadir (FOR 15 and FOR 16) for clear sky over oceans.

The statistics of observed-minus-simulated (O-S) BT differences from CrIS channels flagged as clear for August 27-28 over ocean are shown in Figure 3(a). The biases are primarily contributing from four possible resources, i.e. the numerical weather prediction error, instrument noise, radiative transfer model error, and undetected cloud contamination. Over the window channels in the LWIR (800 to 980 cm^{-1}), there has a 0.2 K negative bias for both day and nighttime. This bias may partially contribute from the cloud contamination in the observations although very restrict cloud detection algorithm is used. The large standard deviation for water vapor channels at MWIR band may mainly come from the ECMWF water vapor forecast field. There is ~1.5 K warm bias existing at the Non-Local Thermodynamic Equilibrium (NLTE) channels (in 4.3 μm CO_2 band) at daytime which is probably from the CRTM NLTE model [Chen et al., 2013a]. The night time warm bias (~0.5 K) for the high peak CO_2 channels (4.3 μm CO_2 band) might due to CRTM error and/or ECMWF temperature forecast field error. However, the root cause is still under investigation. For comparison purpose, the same day O-S from The Infrared Atmospheric Sounding Interferometer (IASI) on MetOp-a/b are shown in Figure 3(b) and 3(c). The IASI is the first operational interferometer in space measuring the 3.5-16.4 μm (645-2760 cm^{-1}) spectrum in 8461 spectral channels with a spectral sampling interval of 0.25 cm^{-1}, which was successfully launched on Metop-a on October 2006 and Metop-b on September 2012, respectively [Hilton et al., 2011]. The IASI observed spectra have been converted to CrIS-alike spectra with CrIS resolution (referred to IASI2CrIS): first applying inverse Fourier transform of the spectra to the interferogram space; then employing the de-apodization with IASI ILS, truncation to CrIS optical path delay (OPD), and apodization with CrIS ILS; and finally applying Fourier transform of the products to spectra space and resampling the spectra on CrIS

resolution. Resampling error from IASI to CrIS resolution is very small (less than 0.02 K) since IASI spectra cover CrIS spectra for all three bands. There is very good agreement between CrIS and IASI comparison with simulation. Note that the smaller standard deviation for CrIS than IASI in band 3 which indicates that CrIS has lower noise in shortwave band.

(a)

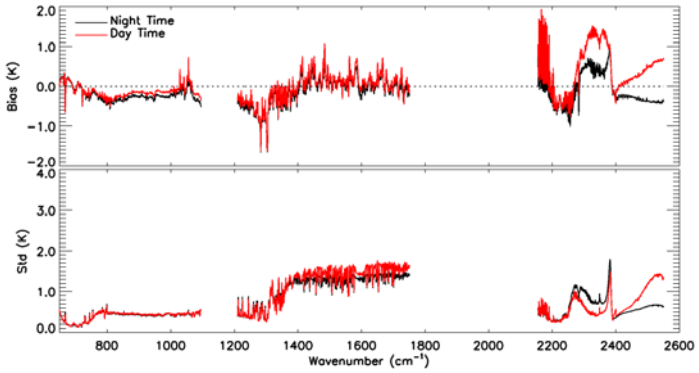

(b)

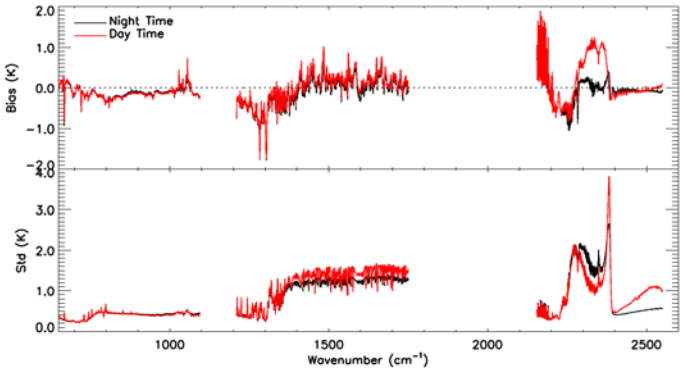

(c)

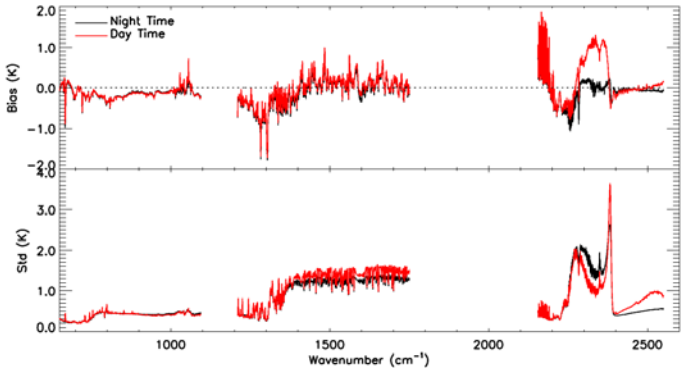

Figure 3. (a) CrIS Observation minus simulation biases (top panel) and standard deviations (bottom panel) for clear sky over ocean. Red curves show the daytime results and black curves show night time results. (b) same as (a) but for results from IASI on MetOp-a. (c) Results from IASI on MetOp-b. The IASI data have been resampled to CrIS resolution.

The detailed CrIS 9 FOVs biases at nadir FOR and standard deviation among their FOVs during night-time are shown in Figure 4. There are large biases at CO strong absorption lines at spectral

range 2155 to 2190 cm^{-1}, which is due to the forward simulations using default climatological CO profile as the CRTM input. The standard deviation among their 9 FOVs is less than 0.2 K except for the very cold channels at 2370-2380 cm^{-1}, which could reach to 0.8 K. The zoomed average biases for all FOVs at CO strong absorption lines within spectral range 2155 cm^{-1} to 2190 cm^{-1} are also shown in this Figure. It shows very good agreement between IASI2CrIS and CrIS at these CO strong absorption lines, even better than the bias with forward calculations. Due to the diurnal variation in the sea surface temperature and local equatorial crossing time difference (CrIS at 13:30 pm and IASI at 09:30 am), the window channels bias difference for CrIS and IASI2CrIS could reach to 0.1 K.

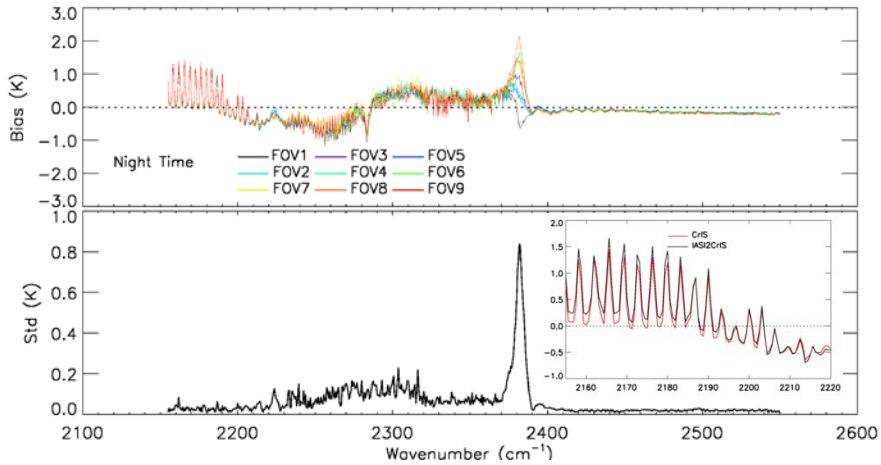

Figure 4. 9 FOVs biases in comparison with CRTM simulations at nadir FOR and standard deviation among their FOVs during night-time. The zoomed average biases for all FOVs at CO strong absorption lines within spectral range 2155 cm^{-1} to 2190 cm^{-1} are also shown with CrIS (red line) and IASI2CrIS (black line).

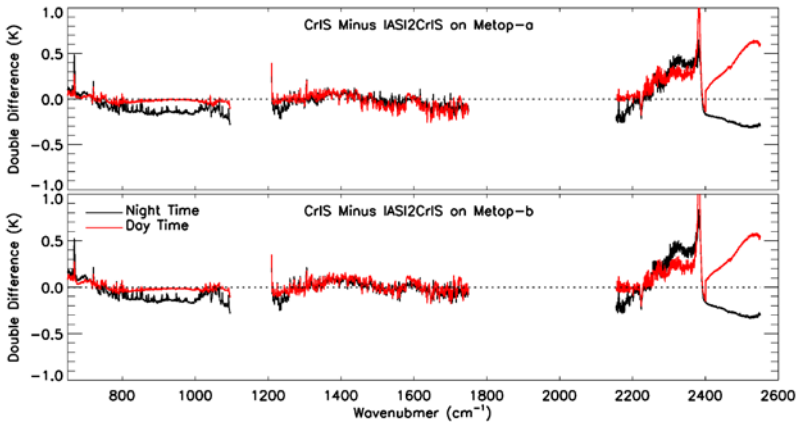

Figure 5. Double difference between CrIS and IASI2CrIS on MetOp-a and MetOp-b during night time (black line) and daytime (red line).

3.2 Double Difference Method

The second assessment approach is calculating the double difference between CrIS and IASI2CrIS on MetOp-a/b using CRTM simulation as a transfer tool for clear scenes over oceans:

$$\Delta BT_{DD} = \overline{(BT_{obs} - BT_{CRTM})_{CrIS}} - \overline{(BT_{obs} - BT_{CRTM})_{IASI\,2CrIS}} \quad (2)$$

S-NPP is in the afternoon orbit with equator crossing Local Solar Time (LST) at 13:30 pm in descending node, while MetOp-a/b are in the early morning orbit with LST at 9:30/8:45 am in descending node. They have a constant time separation of about 4 hours between CrIS and IASI observations. The time difference makes them impossible to meet at the same time and same location at the low latitudes and to make direction radiance comparison, although they can meet at high latitudes at both North and South Pole regions, the so-called simultaneous nadir overpasses (SNO) [Cao et al., 2004]. However, the double difference approach is from a statistical stand point instead of individual comparison. There are several merits for this approach: The forward model only simulates the channel brightness temperatures for CrIS since IASI observations are converted to CrIS-alike radiances, so uncertainty from the forward model can be effectively minimized; The data used to calculate the mean could be very large and represent different atmospheric and surface conditions so that the impact from the observation time difference could be largely reduced; The comparisons can be separated for different times and different locations. The main drawback for this approach is that the diurnal variations in the atmospheric and surface conditions can not completely removed. Figure 5 shows the double difference between CrIS and IASI2CrIS on MetOp-a/b during night time (black line) and daytime (red line). For majority channels, the differences are within ±0.3 K. Excellence agreement could be found at LWIR band during daytime, and MWIR band during both daytime and nighttime. For 4.3 μm CO_2 strong absorption region, CrIS is warmer than IASI about 0.3-0.5 K, which may be contributed by the CrIS lack of nonlinearity correction for SWIR band. For LWIR and SWIR window channels, negative differences about 0.2 K are existed over nighttime. Part of the negative difference about 0.1 K may due to the diurnal variation in the SST, and the other part may due to the possible cloud contamination in CrIS data during night time.

3.3 SNO Method

The third approach is to directly compare the radiance between CrIS and IASI2CrIS with SNO method:

$$\Delta BT_{SNO} = BT_{CrIS} - BT_{IASI\,2CrIS} \quad (3)$$

When a SNO occurs, the radiometers from both satellites view the Earth at the same location and same time from different altitudes, which greatly reduces the comparison uncertainties related to the difference of satellite observational time and viewing geometries. Very strict SNO criteria are applied: time difference is less than 2 minutes; spatial difference is less than 6.5 km, and view angle difference is meeting $abs(\cos(\theta_1)/\cos(\theta_2) - 1) \le 0.01$. An example of radiance comparison between CrIS and IASI on MetOp-a for a SNO event happened at 18:22:22 UTC on 27 August 2013 is presented in Figure 6. We should point out that there are only 7 spectra pairs are collected for this SNO event. Therefore, the results presented here are more qualitative than quantitative. Figure 5 (a) gives the comparison of the mean spectra of paired CrIS (with Hamming apodization) and IASI at their original spectral resolution. Figure 5 (b) shows the

unapodized difference between CrIS and IASI2CrIS. The comparison results indicate that agreement of observations between CrIS and IASI2CrIS is very good for LWIR and SWIR bands, although larger BT difference exists toward the end of SWIR band and for the cold channels in SWIR band.

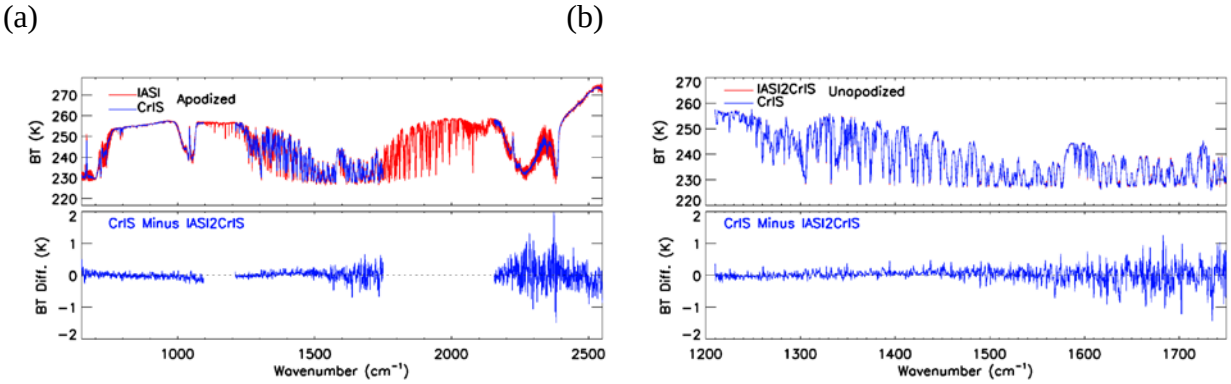

Figure 6. (a) Averaged SNO CrIS and IASI Spectra and difference between CrIS and IASI2CrIS on August 27 2013; and (b) Unapodized CrIS and IASI2CrIS spectra and their difference at MWIR band. Red line for IASI (or IASI2CrIS) spectra, blue line for CrIS spectra.

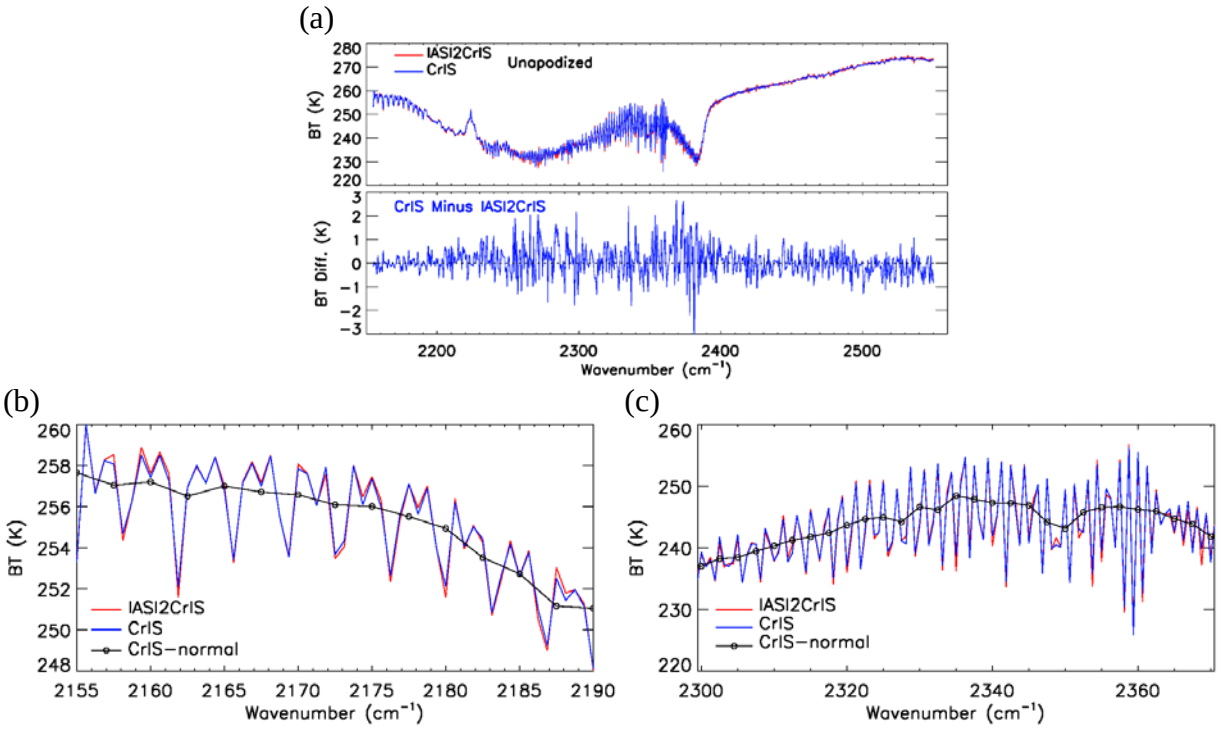

Figure 7. (a) Same as Figure 6 (b) but for SWIR band. (b) and (c) are enlarged plots at the CO absorption lines at the spectral range from 2155-2190 cm^{-1}, and CO2 absorption lines at the spectral range from 2300-2370 cm^{-1}, respectively. The normal mode CrIS spectra are also included.

More detailed comparisons for SWIR band are shown in Figure 7. Figure 7(a) presents the unapodized CrIS and IASI2CrIS spectra and their differences at SWIR band. The zoomed absorption line structures for CO and CO_2 are showed in Figure 7 (b) and (c), respectively. Although there are significant BT differences in this band, the line structures in CO and CO2 regions show excellent agreement between CrIS and IASI. Line structure in CO region (2155-2190 cm^{-1}) provides very good information to retrieve CO amount, which is almost impossible for the normal mode CrIS data due to the lack of line structure with the very coarse spectral resolution of 2.5 cm^{-1}. For the normal mode CrIS data, it is difficult to make spectral accuracy assessment due to the coarse resolution. However, the line structure in CO_2 absorption band (2300-2370 cm^{-1}) in full resolution CrIS data provides very good spectral information to make it feasible to use for spectral calibration in SWIR band.

4. CrIS Spectral Accuracy Assessment

There are two basic spectral assessment methods to evaluation the hyper-spectral satellite sensors [Strow et al., 2006; Strow et al., 2013; Chen et al., 2013b], such as IASI, and CrIS. The first one is the absolute method which requires an accurate forward model such as CRTM to simulate the top of atmosphere (TOA) radiance under clear conditions. It then correlates the observed radiance to the simulated radiance by shifting the spectra at a certain range either from the observation or the simulation to find the maximum correlation. The second method is the relative method. It doesn't need a forward model, only requires two uniform observations to determine frequency offsets relative to each other.

Assuming two spectra S_1 and S_2 with same length and resolution, the correlation coefficient between the two spectra can be written as [Chen et al., 2013b]:

$$r_{S_1S_2} = \frac{\sum_{i=1}^{n}(S_{1,i}-\overline{S_1})(S_{2,i}-\overline{S_2})}{(n-1)D_{s_1}D_{S_2}} = \frac{\sum_{i=1}^{n}(S_{1,i}-\overline{S_1})(S_{2,i}-\overline{S_2})}{\sqrt{\sum_{i=1}^{n}(S_{1,i}-\overline{S_1})^2(S_{2,i}-\overline{S_2})^2}}, \quad (4)$$

where n is the number of channels for each spectrum, $\overline{S}$ and Ds are the mean and standard deviation of spectrum S, respectively. A standard deviation of the difference of the two spectra can be defined as:

$$D_{S_1S_2} = \sqrt{\sum_{i=1}^{n}[(S_{1,i}-\overline{S_1})-(S_{2,i}-\overline{S_2})]^2 \Big/ (n-1)}. \quad (5)$$

The spectral shift factor α, which is defined as $\nu' = \nu(1+\alpha)$ and indicate the stretching (or shrinking) from the original spectrum along the frequency ν, can be efficiently identified by using the correlation method with the maximum correlation coefficient $r_{S(\nu)S(\nu')}$ and minimum standard deviation $D_{S(\nu)S(\nu')}$.

Figure 8 shows the spectral accuracy from the absolute and relative cross-correlation methods for CrIS all three bands. The absolute spectral accuracy is derived using spectra pairs between observations and CRTM simulations under clear sky over oceans, while the relative spectral accuracy is derived using spectra pairs between other 8 FOVs to the center FOV 5. The spectral ranges used to assess the accuracy are the CO2 absorption lines at 710-760 cm^{-1}, water vapor absorption lines at 1340-1390 cm^{-1}, and CO2 shortwave absorption lines at 2310-2370 cm^{-1} for LWIR, MWIR, and SWIR bands, respectively. The relative spectral accuracy relative to FOV 5 is with 1 ppm, and absolute spectral accuracy using CRTM as a truth is within 3 ppm for all three bands. The spectral accuracy from LWIR band 1 and MWIR band are consistent with CrIS normal mode data [Strow et al., 2013]. The excellent spectral accuracy indicates that CrIS instrument has very accurate ILS parameters for the optical alignments and FOV geometry, and that the spectral shifts caused by the self-apodization are effectively eliminated.

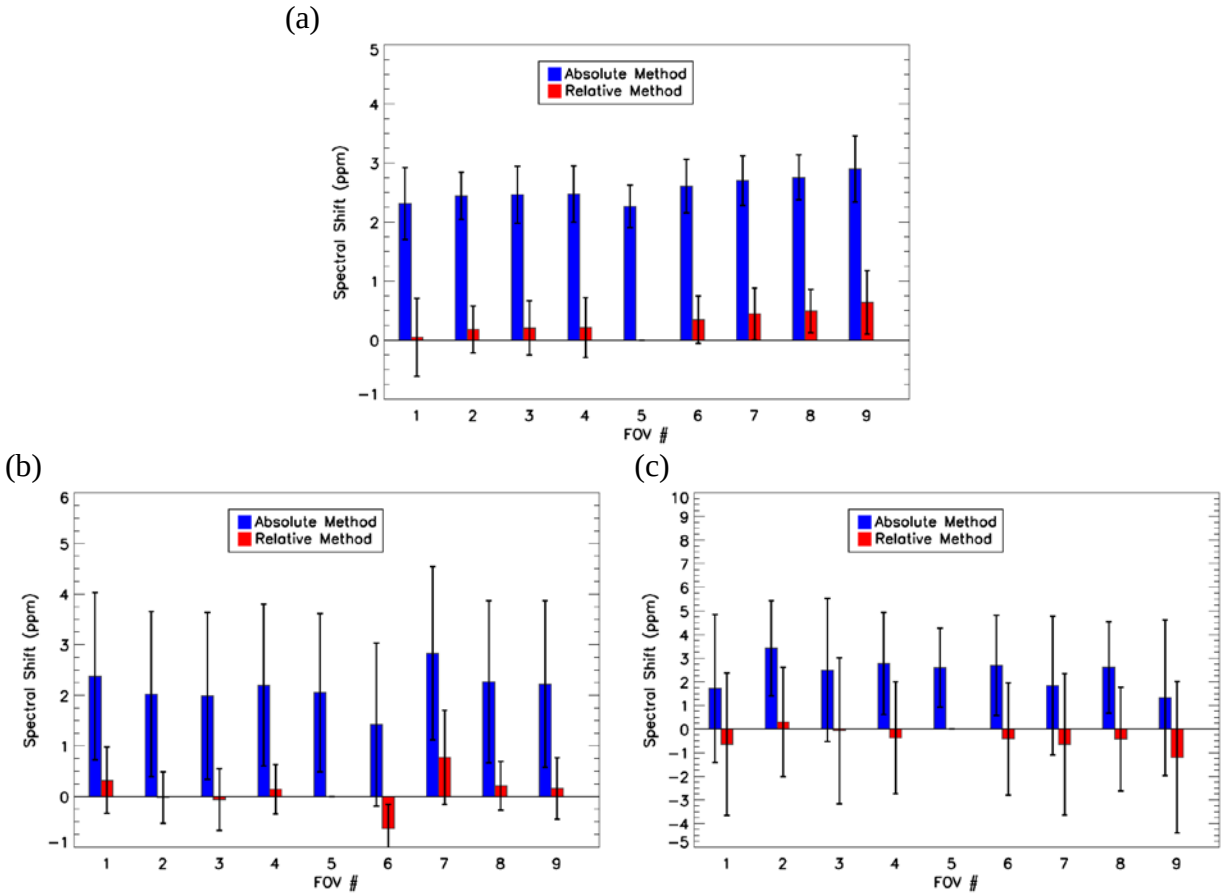

Figure 8. Absolute and relative spectral accuracy of CrIS for all three bands: (a) LWIR band, (b) MWIR band and (c) SWIR band. The vertical bar is the standard deviation.

5. Conclusion

A prototype ADL in full resolution model is developed. Using this model, the CrIS full resolution SDRs are successfully generated offline using the data collected during three in-orbit full resolution experiments. In this study, radiometric and spectral accuracy from the full

resolution SDR data are assessed by using different methods. The following conclusion can be draw based on our analysis:
1) For radiometric accuracy, the FOV-2-FOV radiometric differences are small, within ±0.3 K for all the channels, the double difference with IASI are within ±0.3K for most of channels, and SNO results versus IASI show that agreement is very good for band 1 and band 2, but large BT differences in cold channels for band 3.
2) For spectral accuracry, the spectral shifts relative to FOV5 are within 1 ppm, and the absolute spectral shifts relative to CRTM simulation are within 3 ppm.

Continuous improvements of the radiometric and spectral calibration accuracy of CrIS on S-NPP and JPSS are underway. Once NOAA operates CrIS in FSR mode, the high quality CrIS full resolution SDRs could be generated to support the improvement of water vapor profile in satellite data assimilation systems, and to meet the requirements of improving retrieval accuracy of atmospheric greenhouse gases CO, CO_2, and CH_4 for climate applications.

ACKNOWLEDGEMENTS

This study is funded by the NOAA JPSS Program Office. Yong Chen and Likun Wang are also supported by NOAA grant NA09NES4400006 (Cooperative Institute for Climate and Satellites) at the University of Maryland/ESSIC. The manuscript contents are solely the opinions of the authors and do not constitute a statement of policy, decision, or position on behalf of NOAA or the U.S. government.

REFERENCES

Cao, C., M. Weinreb, and H. Xu (2004), Predicting simultaneous nadir overpasses among polar-orbiting meteorological satellites for the intersatellite calibration of radiometers, *J. Atmos. Oceanic Technol.*, *21*(4), 537-542.

Chen, Y., F. Weng, Y. Han, and Q. Liu (2008), Validation of the Community Radiative Transfer Model (CRTM) by using CloudSat data, *J. Geophys. Res.,* **113,** D00A03, doi:10.1029/2007JD009561.

Chen, Y., Y. Han, P. Van Delst, and F. Weng (2010), On water vapor Jacobian in fast radiative transfer model, *J. Geophys. Res., 115,* D12303, doi:10.1029/2009JD013379.

Chen, Y., Y. Han, and F. Weng (2012), Comparison of two transmittance algorithms in the community radiative transfer model: Application to AVHRR, *J. Geophys. Res.,* **117,** D06206, doi:10.1029/2011JD016656.

Chen, Y., Y. Han, P. van Delst, and F. Weng (2013a), Assessment of shortwave infrared sea surface reflection and non-local thermodynamic equilibrium effects in Community Radiative Transfer Model Using IASI Data, *J. Atmos. Oceanic. Technol.*, 30, 2152-2160. doi: 10.1175/JTECH-D-12-00267.1.

Chen, Y., Y. Han and F. Weng (2013b), Detection of Earth-rotation Doppler shift from Suomi National Polar-Orbiting Partnership Cross-track Infrared Sounder, *Appl. Opt.*, 52, 6250–6257. doi: 10.1364/AO.52.006250.

Han, Y., P. van Delst, Q. Liu, F. Weng, B. Yan, R. Treadon, and J. Derber (2006), JCSDA Community Radiative Transfer Model (CRTM)—version 1, NOAATech, Rep., NESDIS 122, 40 pp.

Han, Y., et al. (2013), Suomi NPP CrIS measurements, sensor data record algorithm, calibration and validation activities, and record data quality, *J. Geophys. Res. Atmos.*, *118*(22), 2013JD020344, doi:10.1002/2013jd020344.

Hilton, F., et al. (2011), Hyperspectral Earth Observation from IASI: Five Years of Accomplishments, *Bull. Amer. Meteor. Soc.*, *93*(3), 347-370, doi:10.1175/bams-d-11-00027.1.

McNally, A. P., and P. D. Watts (2003), A cloud detection algorithm for high-spectral-resolution infrared sounders, *Q. J. R. Meteorol. Soc.*, **129,** 3411-3423.

Strow, L. L., S. Hannon, S. De-Souza Machado, H. Motteler, and D. Tobin (2006), Validation of the Atmospheric Infrared Sounder radiative transfer algorithm, *J. Geophys. Res.*, 111, D09S06, doi:10.1029/2005JD006146.

Strow, L. L., H. Motteler, D. Tobin, H. Revercomb, S. Hannon, H. Buijs, J. Predina, L. Suwinski, and R. Glumb (2013), Spectral calibration and validation of the Cross-track Infrared Sounder on the Suomi NPP satellite, *J. Geophys. Res. Atmos.*, *118*(22), 12,486-412,496, doi:10.1002/2013jd020480.

Tobin, D., et al. (2013), Suomi-NPP CrIS radiometric calibration uncertainty, *J. Geophys. Res. Atmos.*, *118*(18), 10,589-510,600, doi:10.1002/jgrd.50809.

Wu, X., and W. L. Smith (1997), Emissivity of rough sea surface for 8-13 μm: Modeling and verification, *Appl. Opt.*, **36,** 2609-2619.